Atmospheric Research 304 (2024) 107368

Contents lists available at ScienceDirect

Atmospheric Research

journal homepage: www.elsevier.com/locate/atmosres

A 13-year long strokes statistical analysis over the Central Mediterranean area

Marco Petracca [a], Stefano Federico [a,*], Nicoletta Roberto [b], Silvia Puca [b], Leo Pio D'Adderio [a], Rosa Claudia Torcasio [a], Stefano Dietrich [a]

[a] National Research Council, Institute of the Atmospheric Sciences and Climate (CNR-ISAC), Via Fosso del Cavaliere, 100, Rome 00133, Italy
[b] Italian Civil Protection Department (DPC), Via Vitorchiano, 2, Rome 00189, Italy

ARTICLE INFO

Keywords:
Lightning stroke parameters
Ground Network
Strokes statistical analysis
Ground altitude levels

ABSTRACT

This paper presents the first detailed analysis of cloud-to-ground (CG) and intra-cloud (IC) strokes characteristics from the Lightning Detection Network (LINET) over Italy and the Central Mediterranean area, a lightning active area in south Europe. We study the strokes over a 13-year period from 2010 to 2022, aiming to understand how it varies with different temporal scales (hourly, monthly, seasonally, and yearly), surface types (sea and land), and ground levels (0–100 *m*; 100–200 *m*; 200–400 *m*; 400–800 *m*; 800–1200 *m*; 1200–2000 *m* and above 2000 *m*).

We found that the stroke's maximum activity was observed in August; specifically, July has the maximum activity over the land with a maximum diurnal peak in the afternoon, while in September, the convection shifts over the sea with a secondary daily maximum in the morning. The largest current intensities are observed in January, over sea and during nighttime. Moreover we found that stroke current intensities, polarity and IC height emissions are influenced by ground altitude level. Our paper provides new insights into the spatio-temporal patterns and characteristics of lightning over Italy and the Central Mediterranean area, which can be useful for improving weather forecasting, climate modeling, risk assessment, and damage mitigation strategies in this area.

1. Introduction

Lightning is a fascinating and spectacular natural phenomenon, but it is also dangerous and harmful to humans and the environment. Studying the climatology of lightning is crucial for understanding the physical mechanisms that generate it, its relationship to weather and climate, and its impacts on human activities and ecosystems. Lightning is the mechanism by which an electrically charged cloud discharges some of its energy. Lightning is closely related to a multitude of meteorological and climatological aspects: it has been found to be an excellent indicator of global climate change (Reeve and Toumi (1999)), it is linked to the atmospheric pollution in urban areas (Orville et al. (2001); Naccarato et al. (2003)), to the sea surface temperature (Holt et al. (2001); De Pablo and Soriano (2002)), and it is one of the natural sources of nitrogen oxides (NOx) and hence of tropospheric ozone (Nesbitt et al. (2000); Bond et al. (2002); Holler et al. (2009)). Lightning also causes significant structural damage, economic losses, power interruptions and natural forest fires (Wierzchowski et al. (2002)). The annual report conducted by the National Oceanic and Atmospheric Administration's National Weather Service (NOAA-NWS) ranks lightning as the leading cause of deaths each year among convective events (including tornadoes, hailstorms, and storms). In the ranking of deaths caused by weather-related events (Curran et al. (2000)), lightning is second only to floods. Lightning fatality rate in Europe in the 20*th* century was on the order of 0.3 deaths per million per year as reported by the annual rates of lightning fatalities by country (Holle (2008)). The strong correlation observed between lightning and convective precipitation (Petersen and Rutledge (1998); Deierling et al. (2008)) further fuels interest in this atmospheric phenomenon. Roberto et al. (2016) and Sokol et al. (2023) have also observed from meteorological radar measurements in thunderclouds a high correlation between the number of lightning strokes and the mass and size of the hydrometeors in the ice phase.

The interest in lightning is stronger than ever, as confirmed by the numerous satellite missions planned with an on-board sensor for lightning observation, such as the GOES-R launched in November 2016 with

* Corresponding author.
E-mail address: s.federico@isac.cnr.it (S. Federico).

https://doi.org/10.1016/j.atmosres.2024.107368
Received 11 October 2023; Received in revised form 12 March 2024; Accepted 23 March 2024
Available online 31 March 2024

the Geostationary Lightning Mapper (GLM) or the Lightning Imager (LI) on board the third-generation European MeteoSat (MTG) satellite launched last December 2022. There are also a number of ground-based lightning detection networks that are becoming increasingly dense, using the electromagnetic properties of lightning to detect its geolocation and other physical quantities. Most networks are limited to specific countries, such as PERUN in Poland, ALDIS (Austrian Lightning Detection and Information System), RINDAT (Brazilian Lightning Detection Network), SALDN (South African Lightning Detection Network), NLDNs (US and Canada National Lightning Detection Networks), and CESI in Italy, to name a few.

Other networks have a wider spatial coverage, such as ATDnet (Anderson and Klugmann (2014)), National Observatory of Athens ZEUS detection system (Kotroni and Lagouvardos (2008)) spread across Europe, or EUCLID (Schultz et al. (2016)), a consortium founded in 2001 that has over 180 sensors in Europe and has been extensively analyzed in various studies (Piper and Kunz (2017); Mohr et al. (2019); Taszarek et al. (2019); Manzato et al. (2022)).

Each network has its own peculiarities and intrinsic detection capabilities depending on the type of electromagnetic frequencies used (Very High Frequencies (VHF) or Very Low/Low Frequencies (VLF/LF)), requiring intercomparison studies to ascertain and identify the potential of each network.

VLF and LF radiation is produced by lightning processes ranging from long-duration continuing currents (from several tens to hundreds of milliseconds) to relatively short-duration currents (few to tens microseconds) flowing through cloud and cloud-to-ground lightning channels. The VLF/LF generally locates the signals emitted by the latter processes, which include the return stroke in the CG discharges and other relatively high amplitude pulses radiated mainly by vertical channels in the cloud. On the other hand, VHF radiation from cloud and cloud-to-ground lightning is associated with the breakdown of virgin air as part of the channel formation process and leader processes in pre-existing channels.

Networks operating in the VLF/LF ranges are generally referred to as "long-range" networks because the electromagnetic radiation from lightning is the most powerful in this frequency range and the signals typically have wavelengths in the range of 10–100 *km* and propagate through the Earth-ionosphere waveguide, such that they can be measured by sensors at distances of a few thousand kilometers from the location of the lightning process. On the other hand, networks operating in VHF are referred to as "short-range" because the electromagnetic radiation from lightning in this frequency range has wavelengths of approximately 1–10 m and must be measured by sensors within the line-of-sight distance of lightning process. As a result, various types of networks offer complementary storm information, necessitating the use of different techniques to assess or validate the performance characteristics of distinct sensors (Nag et al. (2015)).

Different studies on thunderstorms' climatology have been based on lightning detection networks at different scales: national, continental, or global (Pohjola and Mäkelä (2013); Virts et al. (2013); Wu et al. (2016); Galanaki et al. (2018); Zhang et al. (2018); Xu et al. (2022)). Many analysis are evaluated over the Mediterranean Sea, which is one of the major centers of electrical activity during the Northern Hemisphere winter (Christian et al. (2003); Kotroni and Lagouvardos (2008)). Kotroni and Lagouvardos (2016) have studied the relationship between lightning and sea surface temperature in the Mediterranean Sea. Galanaki et al. (2016) utilized a decade-long dataset from the ZEUS network to analyze lightning and Mediterranean cyclones, Poelman et al. (2016) used an 8-year dataset (2006–2014) from EUCLID to study climatology in Europe, Cacciamani et al. (1995) analyzed the thunderstorm climatology in northern Italy using SYNOP data, Feudale and Manzato (2014) examined the distribution of cloud-to-ground (CG) lightning in relation to the orography and to the anthropogenic emissions in Northern Italy.

However, these studies focused on CG flashes and limited their analysis to Northern Italy. This study presents, for the first time, the 13 years long-term statistical analysis (from 2010 to 2022) of lightning using a highly sensitive network across a large area of almost 1.5 million km^2, which includes the entire Italian peninsula, parts of neighboring European countries, and part of the Mediterranean Sea (red box in Fig. 1). Italy serves as an ideal testing ground for complex terrains within the Mediterranean climatic regime, encompassing a blend of mountainous landscapes (Alps, Apennines) and more level/coastal regions (Petracca et al. (2018)).

In this work we use the LINET network, which is a VLF/LF network deployed throughout Europe and it is also present in other continents such as South America, Australia, and Central Africa (Betz et al. (2009); Holler et al. (2009)). The network distribution shows a high sensitivity in detecting currents well below 2 *kA* over most of Italy and surrounding countries, as shown in Section 3.1, and can be used for a comprehensive study on total lightning, offering detailed analysis on a large scale beyond individual countries and extending internationally (Betz et al. (2004)). The network allows for a comprehensive study of both IC and CG strokes, along with their individual characteristics such as discharge intensity, polarity, IC altitude, as well as the number and density of lightning events. Each parameter is statistically analyzed based on its spatial and temporal distribution. The objective is to study the statistical characteristics of lightning strokes in the Mediterranean area, and identify new and interesting relationships between lightning physics and spatio-temporal interconnections. The entire analysis is based on a single database that collects, organizes, classifies, and relates the strokes recorded by the lightning detection network in near real time (NRT).

The paper is organized as follows: in Section 2 a comprehensive description of the LINET network and the applied methodology are presented to characterize the lightning spatial and temporal distribution. Then, a detailed discussion and description of the results obtained on the long-term statistical analysis of strokes is described in Section 3 following the applied methodological approach. Lastly, Section 4 summarizes the conclusions of this work. Finally, Appendix A describes the database developed and used to retrieve all results shown here.

2. Material and Methods

2.1. LINET network

The ground network is designed with a modular approach, consisting of three modules. Module 1 utilizes two crossed loops as a passive sensor for magnetic field components, eliminating the need for active electronics. Module 2 incorporates a GPS clock for precise signal timing. Module 3 handles signal amplification, filtering, AD-conversion, and data processing.

The international European network started operation on 1*st* May 2006, even if it is not homogeneously distributed. Data collected by each sensor are transmitted to the central station in Munich, Germany. The concept aims at a baseline of 150–200 *km* in order to enable 3D discrimination between CG and IC, reasonably well fulfilled within Central Europe, but some areas await completion and expansion of the network geometry. Sampling rate is set at 1 MHz with 14-bit resolution, and triggered events are processed with minimized data loss or rearm time. Technical noise signals are largely reduced through Fourier analysis and time coincidence considerations.

In areas where distance from sensors is over 200 *km*, i.e. over the sea, the Detection Efficiency (DE) decreases so that only stronger strokes can be detected; still, storms can be identified far away and traced over long paths. The DE is defined as the ratio between actually reported and really existing strokes. Determining the absolute value of the DE of a network as LINET is a difficult task, as requires specific experiments and comparison with other networks for the investigated area, and only estimates can be given in the context of this paper. Since the sensor sensitivity and the implemented location algorithm are fixed, the final DE depends on the network geometry and exhibits spatial variations (Aranguren et al. (2014, 2017)). The LINET network reaches a high DE

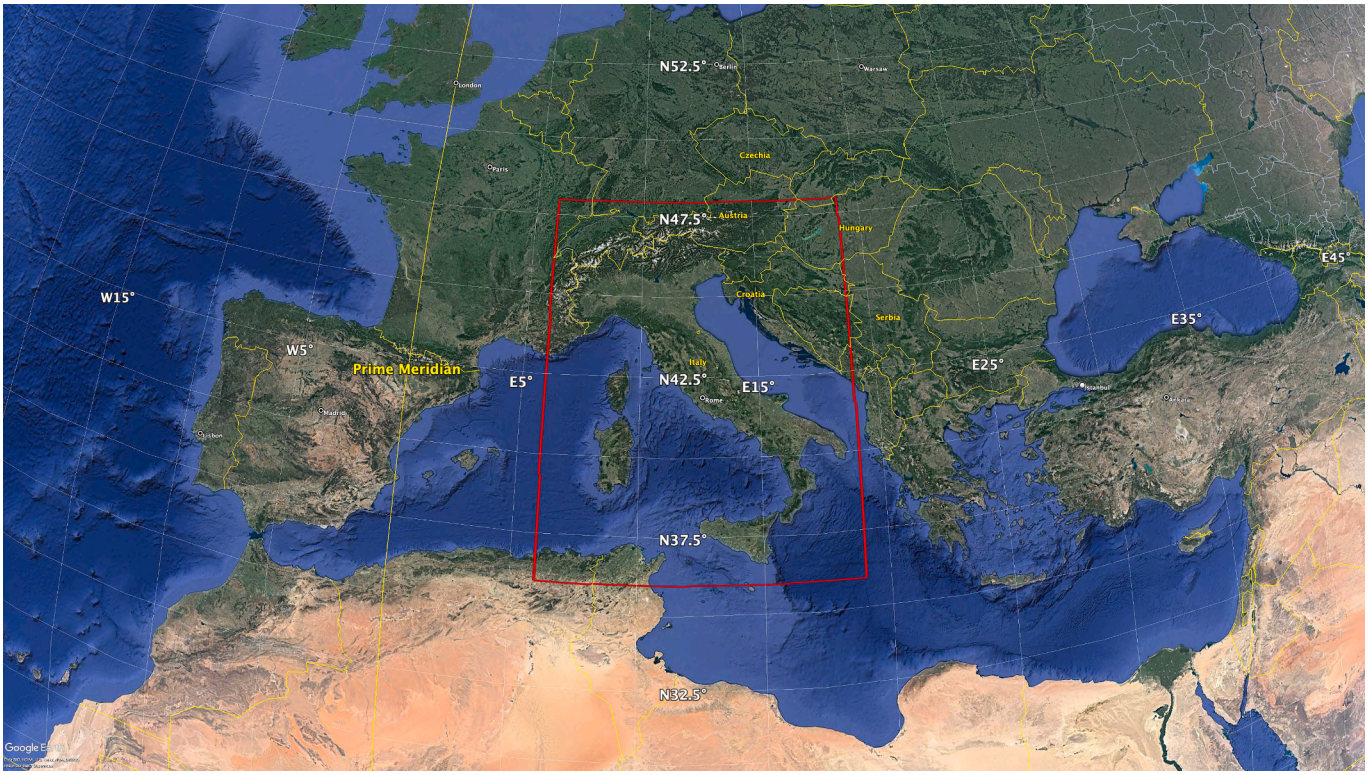

Fig. 1. The red rectangle limits the area of analysis. (For interpretation of the references to colour in this figure legend, the reader is referred to the web version of this article.)

as it detects strokes with current intensity even below 1 *kA* (see Fig. 6). A rough estimation of the LINET DE can be done using the methods of DE estimation in Diendorfer et al. (2009). In particular, using the "reference" intensity distribution of Diendorfer et al. (2009), also shown in Aranguren et al. (2014) in their Fig. 4, for a minimum current of 4 *kA* the 95% DE is expected, while for a minimum current of 2 *kA* the 99% DE is expected. As shown in Section 3.2, the minimum current of 2 *kA* is detected in 60% of the domain investigated in this paper, and minimum currents are below 4 *kA* for 85% of the domain. So, the DE is expected larger than 95% across the network.

ICs exhibit a frequency spectrum that overlaps significantly with the one from CG return strokes. Thus, all VLF/LF networks measure necessarily both stroke types. IC-CG discrimination is achieved using a 3D-algorithm, which doesn't rely on the wave-form, signal amplitude, and polarity. The 3D-algorithm, however, depends on the geometry of the network and the discrimination becomes reliable if the distance among sensors is <250 *km* (Betz et al. (2004)). In this way, the strokes are <120 *km* from the nearest sensor, and this guarantees that the time of arriving (TOA) difference between emission of IC and CG remains larger than the statistical timing error. This 3D-TOA method gives accurate estimation of the vertical position of IC strokes with an error of 500 *m* (Aranguren et al. (2017)). This error, however, can increase to 1–3 *km* depending from statistical distributed GPS time errors, or site errors specific to the conditions around each station (like ground conductivity or orography), or from complex pulse shapes or other reasons (Holler et al. (2009)).

The horizontal location accuracy is approximately 150–300 *m*, verified by means of strokes to towers. This high location accuracy is reached by the feature to pin down the arrival time of incoming stroke signals with an average accuracy of 200 *ns* (Betz et al. (2009)).

It is important to note that the deployment of the LINET network over Italy has distances between the sensors which are farther than 250 *km* in some areas, especially in Southern Italy and over the Tyrrhenian Sea. This implies that the network capability to distinguish CG and IC strokes is reduced in these areas. In particular, Holler et al. (2009) reported the analysis of the ratio between IC and CG in several parts of the world (Australia, Africa, Europe, South America) and, even if there is a variability of the results in the different countries, the IC fraction ratio is larger than 0.6 (i.e. 60% of the total strokes recorded are intra-cloud strokes). The IC fraction for our case, not shown, is larger than 0.6 for some areas with a typical dimension of 30–40 *km* around each receiver. This fraction, however, decreases rapidly out of these areas showing that the specific geometry of the network over Italy, does not allow for a complete discrimination between IC and CG strokes out of these areas. As in this paper we are interested to examine the general characteristics of the total lightning over the whole Italy and surrounding areas, we show some general characteristics of the IC pulses, as their currents, polarity, or altitude frequency, without considering any result regarding their spatial distribution. However, the IC characteristics shown in this paper help to highlight some important aspects of the convection over the area.

The CNR-ISAC in Rome receives lightning stroke data in NRT, minute by minute, over the Italian area. Specifically, the data covers an area of almost 1.5 million km^2, namely between 36 and 48°N, and 6 and 19°E with approximate dimensions of 1110 *km* in longitude and 1300 *km* in latitude (Fig. 1). From January 1*st*, 2010, until the end of 2022, a period of 13 full years, >6.8 million files have been stored. These files contain a total of >165 million recorded strokes. An overview of the Database (DB) structure is reported in Appendix A.

2.2. Methods

Italy presents a unique orographic complexity in the global panorama. Being narrow and long, it extends for hundreds of kilometers into the Mediterranean Sea, with a roughly 3000 *km* long backbone formed by the Apennine Mountains running from north to south. It boasts approximately 8000 *km* of coastline with highly pronounced variations in altitude, transitioning rapidly from sea to mountains within a few kilometers. Given the considerable variation in land elevation, this study

classifies the land and sea areas separately, using a defined coastline as the dividing line (see Table 1). For the land areas, a further sub-classification into 7 different terrain elevation levels (here after named ground levels) has been performed (Table 2 and Fig. 2).

The grid used is regular with a resolution of 0.1° in latitude and longitude, resulting in a total of 120 (in latitude) x 130 (in longitude) grid boxes (GB). Each GB is associated with a terrain elevation value obtained from the high-resolution Digital Elevation Map (DEM) GTOPO30. As shown in Table 1, the number of GBs is evenly distributed between land and sea, accounting for 46.87% and 47.76%, respectively, the remaining 5.37% GB being the coastline. Regarding the classification based on ground levels (Table 2), there is a slight disparity in favor of the central levels: hilly areas (200–800 *m*) predominate, followed by plains (0–200 *m*), and mountains (800–2000 *m*) with altitudes above 2000 *m* rank last in terms of area extension. The spatial distribution of all GBs, defined as sea areas, coastlines and ground levels over land areas, is shown in Fig. 2.

The statistical analyses conducted on the strokes and their characteristics were carried out evaluating the number and current intensity of both IC pulses and CG strokes, as well as the discharge altitude for ICs. The statistical analyses were conducted in relation to temporal information, classifying the characteristics on yearly, monthly, seasonal, and daily basis, as well as in relation to spatial information, based on the type of surface (land or sea) or the ground level. Furthermore, more in-depth analyses were also performed by intersecting spatial and temporal information. Results are presented from the yearly analyses to the finer temporal scales (i.e. hourly daily analyses) for all spatial classifications and parameters under examination. The combination of these analyses is described in the following section.

3. Results and discussion

3.1. Overall analysis

The lightning strokes dataset contains important information to extract different climatological features of the lighting in the selected Mediterranean area, such as the distinction between IC and CG strokes, their emission altitudes, and different current intensities.

As stated in Section 2.1, the accuracy to discriminate IC and CG strokes is related to the distance from the sensors. This factor affects the measurements of ground-based networks and becomes particularly significant in areas like the Italian peninsula, which is surrounded by the sea and traversed by the long and narrow mountain range of the Apennines. Therefore, in this study, we analyze IC and CG strokes without distinction based on surface type. Nonetheless, we consider the current intensity measurements and the estimation of discharge heights of all identified IC pulses to be sufficiently reliable and worthy of in-depth analysis.

Fig. 3 shows the analysis of the current intensities of all strokes, also divided by type of discharge and polarity. Both IC and CG stroke distributions have a peak in current intensities between 3 and 4 *kA* (Fig. 3a). CG strokes are more numerous in the higher intensity classes, prevailing on ICs from 8 *kA* and above. IC pulses have a lower current intensity variability compared to CG strokes. IC pulses have predominantly positive current intensities (in 53% of cases), while CG strokes are predominantly negative (in 60% of cases). In fact, the median values reveal a slightly positive value of +2.2 *kA* for ICs and a negative value of −3.8 *kA* for CG strokes (Fig. 3b).

Table 1
Surface type classification. Percentage of grid boxes of domain (GB).

Surface type	Altitude [*m*]	GB (% domain)
Sea	≤ 0	7451 (47.76%)
Land	> 0	7311 (46.87%)
Coast	boundary line	838 (5.37%)

Table 2
Ground level classification.

Ground level	Altitude [*m*]	GB (% domain)
Low plain	≤ 100	844 (5.41%)
High plain	(100–200]	1025 (6.57%)
Low hill	(200–400]	1323 (8.48%)
High hill	(400–800]	1824 (11.69%)
Low montain	(800–1200]	1026 (6.58%)
Medium montain	(1200–2000]	880 (5.64%)
High montain	> 2000	389 (2.49%)

Positive CG strokes are, on average, weaker (median value of +5.1 *kA*) and have a limited range (the central part of the distribution spans within 4.4 *kA*, ranging from +3.6 *kA* to +8.0 *kA*) (Fig. 3d). Typically, positive CG are stronger than negative CG, and this results is likely determined by the difficulty to discern between IC and CG strokes. Indeed, positive IC strokes could have be misclassified as positive CG determining the low current of positive CG strokes. On the other hand, negative CG strokes generally have higher intensities with a median value of 7.8 *kA* and greater variability. Both positive and negative CG strokes exhibit a frequency peak between 3 and 4 *kA* (Fig. 3c). The peak is more pronounced for positive discharges (blue), which are predominantly found at lower intensities. In contrast, negative discharges (red) display a longer tail in the distribution curve and a greater occurrence of high intensities.

The emission altitudes of the electrical discharges identified for all IC pulses shows the peak of the distribution between 6.5 and 8 *km* (Fig. 4). There is no significant difference observed between positive and negative polarities (not shown).

Summarising, the results show that ICs are less intense than CG strokes and show a higher occurrence of positive discharges. They have an altitude which peaks at 7 *km*, well in line with the heights of convective thunderstorms over Italy (Buiat et al. (2017); Roberto et al. (2016)).

3.1.1. Spatial distribution

This section presents the spatial distribution of the analyzed stroke parameters on a regular grid. These parameters include stroke density, emission altitude, and current intensities.

All stroke data collected over 13 years have been aggregated into a grid consisting of 120 × 130 GBs (Fig. 5). Each GB has a size of 0.1° in latitude and longitude, equivalent to approximately 10*km* × 10*km*, covering an area of around 100 km^2. The average observed stroke density is approximately 8.14 strokes per km^2 per year. The highest annual mean value, reaching 41 strokes per km^2, is observed along the Montenegrin coastline (42.35°N; 18.85°E).

The number of strokes ranges from a few hundred to over 50,000 strokes per individual GB. There are no areas within the analyzed domain without strokes. The areas with the lowest number of strokes are those over the sea, particularly in the vicinity of North Africa. In these areas, the distance from the network sensors is such that the DE significantly decreases. Over land, it is the Alpine chain that records a lower number of lightning strokes compared to the surrounding zones. In this case, the complex orography of the area may decrease the LINET DE. However, as shown in Aranguren et al. (2014, 2017) the decrease of the DE for an even more complex area than that investigated in this paper, is less that 20%, so the minimum along the peaks is the results of the lower electrical activity in the region, more than an artifact of the DE of LINET.

In Italy, the Ligurian coast and the Tuscan plain near the Tyrrhenian Sea stand out in terms of stroke frequency. This result differs from findings in other studies (Manzato et al. (2022)), where the northeastern part of Italy was identified as the most electrically active area. This discrepancy is likely due to the differing in sensor density across different regions. The EUCLID lightning detection network, for example, utilizes more sensors in northeastern Italy but lacks sensors in the

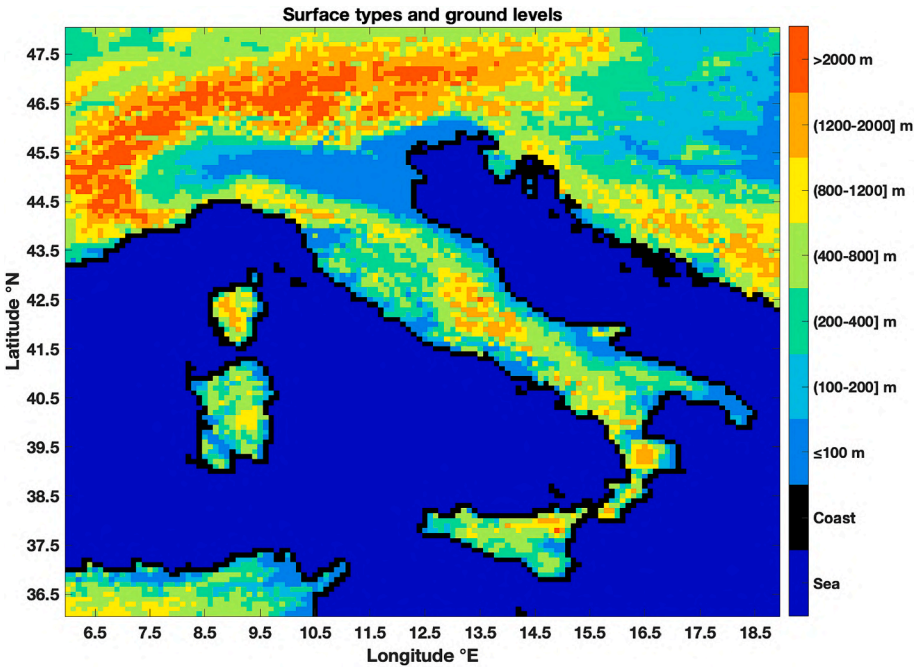

Fig. 2. Spatial distribution of surface types and ground levels.

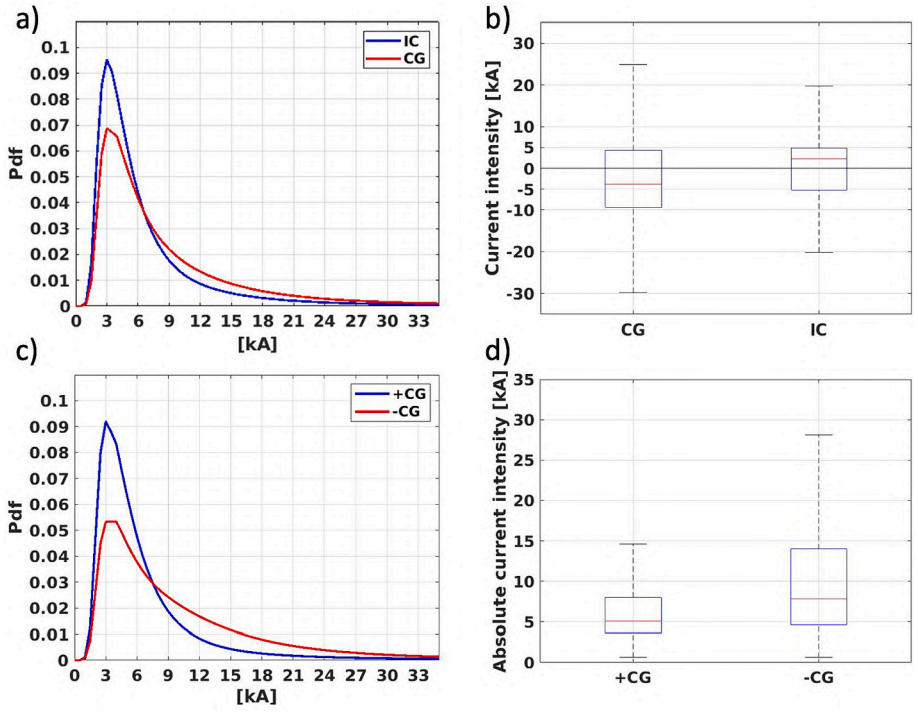

Fig. 3. Analysis of strokes current intensities. IC and CG intensities are shown as PDFs (probability density function) in panel **a**, as boxplot in panel **b**; +CG and -CG intensities are shown as PDFs in panel **c**, as boxplot in panel **d**. The sampling rate in PDF is 0.5*kA*. In each box the central red mark indicates the median, and the bottom and top edges of the blue box indicate the 25*th* and 75*th* percentiles, respectively. (For interpretation of the references to colour in this figure legend, the reader is referred to the web version of this article.)

Ligurian area. From a meteorological point of view, the maxima over Tuscany and Liguria are caused by the uplift of humid air masses from the sea over the local orography and by the fact that the two regions are well exposed to storms incoming from the Western Mediterranean and to storms generating over the Genoa Gulf (Flaounas et al. (2022)).

Feudale and Manzato (2014) and Manzato et al. (2022) results show a high strokes number in the lower Alps and pre-Alps. This is in agreement with our analysis, and it is consequence of the thunderstorms that develop in the lower heights of the Alps, and then propagate Eastward and NorthEastwards following the main circulation, which is usually from West to East. These thunderstorms may originate from several con-causes: destabilisation of the planetary boundary layer in a potentially unstable atmosphere, orographic forcing that constrain the humid flow from the Adriatic Sea to ascend, mountain-valley flow

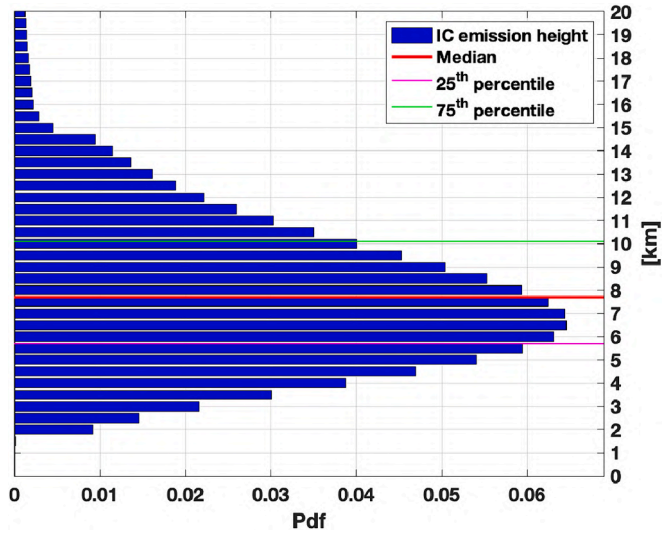

Fig. 4. Pdf of the emission altitudes of the electrical discharges for IC pulses, with a sampling size of 0.5*km*. The x-axis represents the probabilities of occurrence for each altitude, normalized with respect to the total number of ICs detected. Median value, 25*th* and 75*th* percentile values are also indicated.

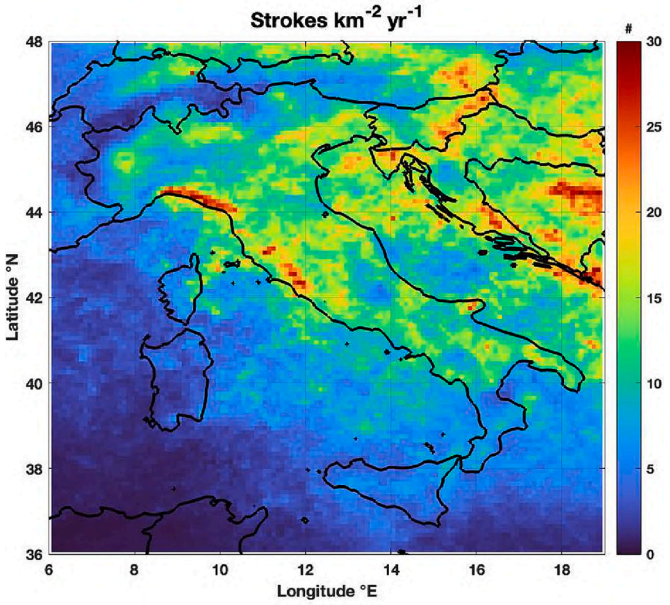

Fig. 5. Spatial distribution of LINET strokes recorded between 2010 and 2022 expressed in terms of average number of strokes per square kilometer per year.

(Federico et al. (2000)), convergence along dry lines or the passage of a synoptic-scale storm. Especially, the destabilisation of the planetary boundary layer and breeze circulations can trigger thunderstorms in summer.

Another area of intense lightning activity is the Northern Adriatic Sea. This relative maximum is caused by two main factors: the advection towards the sea of thunderstorm originated over the Italian mainland (Torcasio et al. (2023)) and the convection developing locally. While the first factor is very important in summer, the second is more important in other seasons, as better explained in section 3.2.2.

Our analysis, shows an intense convective strokes activity along the Apennines that propagates in both eastern and western directions, easily reaching the coastal areas. An exception to this feature is the Calabria region, the southernmost tip of the Italian peninsula, which is less interested by thunderstorms compared to the rest of the peninsula. Interestingly, and despite the largest amount of rain is recorded on the west side of Calabria, the number of lightning are larger on the eastern side of the region, especially southeastern side of Calabria, where the most intense convective activity occurs (Federico et al. (2009); Avolio and Federico (2018)).

The analysis on the spatial distribution of the intensity of the strokes minimum current (Fig. 6) is useful for better understanding the strokes density analysis. Our results show an increase of the minimum currents going westwards and towards the southern portions of the domain. This increase is determined by the lower sensitivity of the LINET network in these regions because they are distant from the sensors, and the LINET DE is lower in these areas. Despite of this issue, Fig. 5 shows a significant electrical activity over the Tyrrhenian Sea, which will be further explored in Section 3.2.2. It is also important to note that the DE of the LINET over the sea close to the Italian mainland, and over the Adriatic Sea, is comparable with that over the land.

Before concluding this section it is important to recall some properties of the DE of LINET that have been already used and will be used in the following: a) the DE of LINET over the domain considered in this paper is expected high (> 95% over 85% of the domain, corresponding to the isoline of minimum current of 4 *kA*). In the paper of Holler et al. (2009), the area of minimum current detection of 2 *kA* was used to identify the regions with a very high DE (~ 100% DE). This minimum current is detected over 60% of our domain; b) The DE over the Adriatic Sea is in line with that over the land and specific analyses can be done in this portion of the sea and compared with the results over the land, the comparison being not influenced by different LINET DE; c) The DE doesn't show important variations between the mountains, including the Alps, and the lowlands.

The results discussed in this section extend the finding of the previous studies because the analysis covers a wider domain. Among the new findings there are the lightning activity over the Tyrrhenian Sea and southern Italy, the extension of the convection over the whole Italian peninsula, and the extension of the convection over the southern part of the Adriatic Sea.

3.1.2. *Surface type-based distribution*

Let's further analyze the spatial distribution of the strokes by

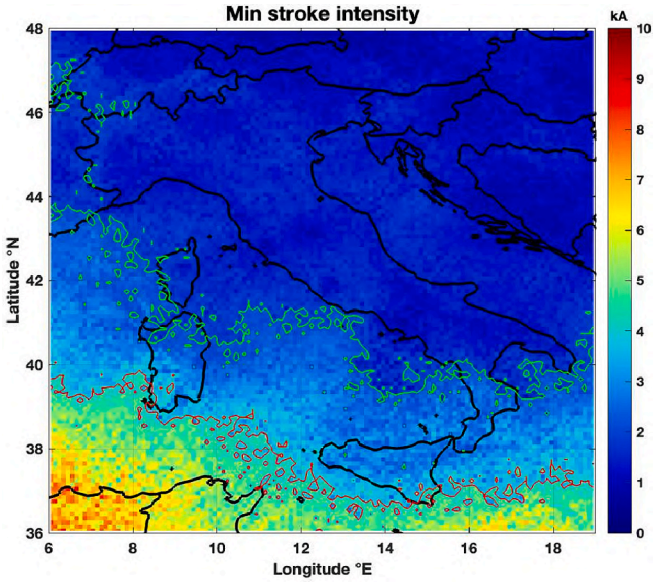

Fig. 6. Spatial distribution of recorded minimum current intensities (threshold). Isolines for 2 *kA* (green line, roughly corresponding to the 99% DE) and 4 *kA* (red line, roughly corresponding to the 95% DE) are also indicated. (For interpretation of the references to colour in this figure legend, the reader is referred to the web version of this article.)

classifying the entire domain into two different surface types (namely "Sea" and "Land") as shown in Table 1. Examining the total number of strokes recorded in each surface type, it is apparent that the majority of electrical discharges are detected over land (59.6%, with an average annual density of 10.4 strokes per km^2 per year). Approximately 34.6% of the strokes are recorded over the sea (with an average density of 5.9 strokes per km^2 per year). The remaining 5.8% are strokes recorded along the separation line between land and sea areas (coastline). The figures of this paper representing the differences between the sea and the land neglect the strokes along the coastline for readability. However, strokes along the coastline show a behaviour that is between the strokes over the land and those over the sea. The differences between strokes over the land and over the sea is more apparent analysing the currents intensities, which show higher values over sea, with an average of 12.2 *kA*. It is interesting to note that the most intense electrical discharges were recorded over sea during the 13 years of detection: +545 *kA* for the strongest positive discharge and − 615 *kA* for the strongest negative discharge. Over the land, discharges are weaker, with an average current of 8 *kA* and minimum values of 0.5 *kA*.

This could be in part explained by the lack of the sensors over the sea, however we believe that this result is a consequence of the difference between the convective clouds over the land and over the sea. For this purpose, we considered the characteristics of the strokes over the Adriatic sea, North of 41°*N*, where the minimum stroke intensity is lower and the DE of LINET is high (Fig. 6) and comparable with the DE over the land. The density of the strokes over the Adriatic Sea (12.5 str per km^2 per year) is slightly higher compared to the land (10.4 str per km^2 per year) confirming the good DE of the LINET network over this portion of sea. The median current of the strokes over the Adriatic Sea is 9 *kA*, which is larger than the median current over the land (8 *kA*) confirming that strokes over the sea tend to be more intense than strokes over the land. Similar results have been found in other studies (Poelman et al. (2016)).

3.1.3. Ground altitude-based analysis

We focus the attention on strokes that occur over mainland, leveraging a network characterized by consistent and optimal reliability across the entire territory. An analysis related to the ground altitude (i.e., seven ground levels according to Table 2) has been carried out. Each panel in Fig. 7 displays the variation of two different parameters with terrain altitude. In the first panel (Fig. 7a), the trend of stroke density, expressed in the number of strokes per km^2 per year, is depicted in blue (with reference to the left y-axis) for the 7 ground levels indicated on x-axis, while the occurrence of negative CG strokes is reported on the right y-axis (in orange). A higher density of strokes is observed at lower altitudes. As the altitude increases, a decrease in stroke density is

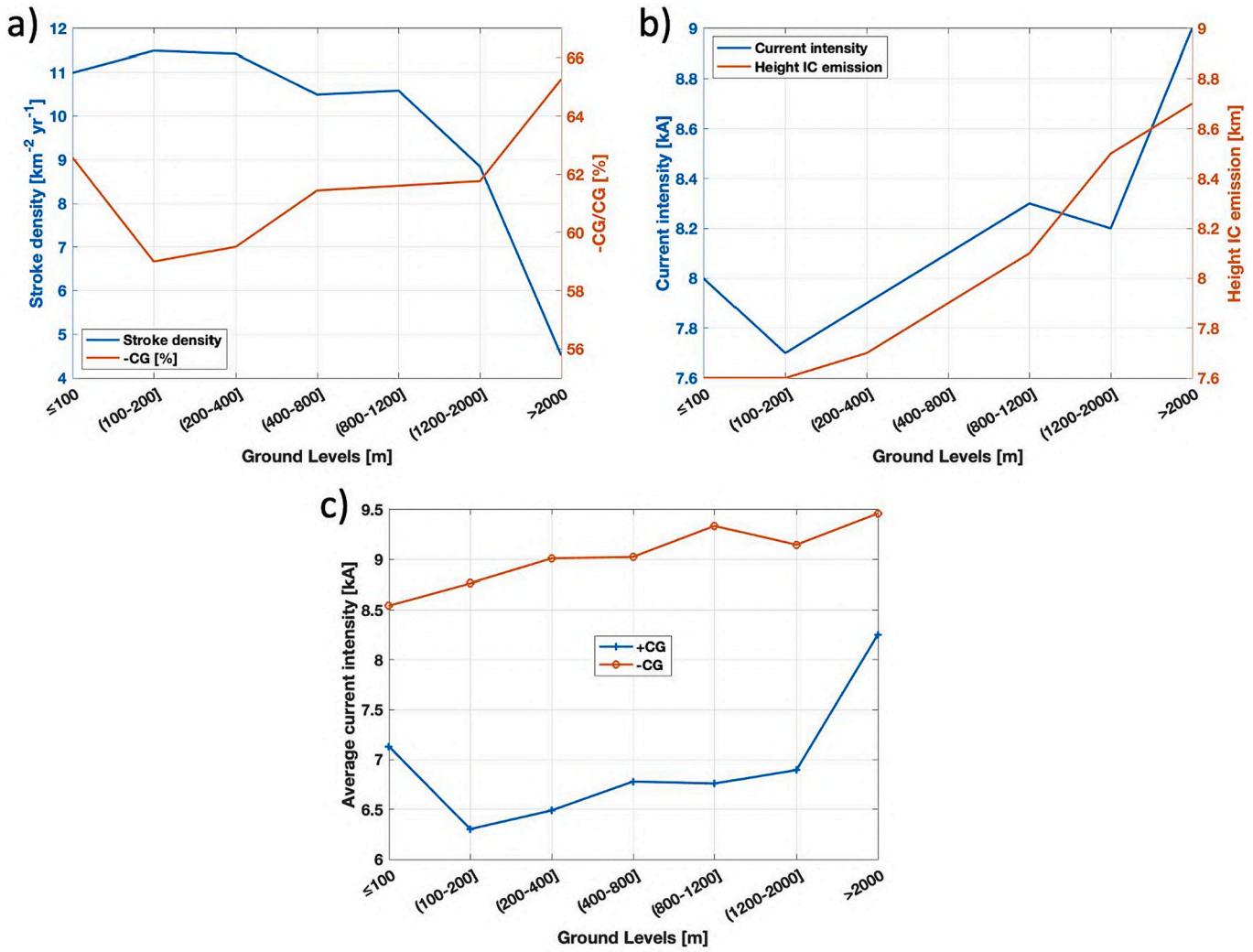

Fig. 7. Trends of stroke parameters across the 7 ground levels. In panel **a** are shown the average stroke density (blue) and the percentage of negative CG strokes (orange); in panel **b** the average current intensity of strokes (blue) and the average altitude of IC emission (orange); in panel **c** the average current intensity for +CG (blue) and -CG (orange) strokes. (For interpretation of the references to colour in this figure legend, the reader is referred to the web version of this article.)

noticeable, reaching a minimum of 4.5 str/(km^2 yr) for ground levels exceeding 2000 *m*. Part of this decrease could be caused by the lower DE of the LINET network in complex orographic areas.

While stroke density is lower in high mountain areas compared to the lower altitudes, the majority of CG strokes recorded above 2000 *m* altitude have negative discharge: 65% of CG strokes are negative in the higher mountains. The trend of the -CG strokes occurrence shows a constant increase from lower to higher altitudes, with values ranging between 59% and 65%. Across the entire dataset, the mean occurrence of -CG strokes is 60%.

In the second panel of Fig. 7b, we show the variation of the average altitude of IC emission with the terrain. The altitude of the IC discharge increases continuously from 7.6 *km* in flat terrain to 8.7 *km* in high mountain areas. This behaviour is, at least partially, explained by the orographic forcing, which facilitates the development of deep cumulonimbus clouds.

Furthermore, in Fig. 7b, the intensity of the electrical discharge as a function of the terrain altitude is shown in blue. There is a clear trend with respect to the terrain altitude: in general, as the altitude increases, the intensity of the discharges gradually increases, reaching up to 9 *kA* in high mountain areas. The weakest intensity values, around 7.7 *kA*, are recorded in hilly areas between 100 and 200 *m* of altitude (Aranguren et al. (2014, 2017)).

Interestingly, we note a decrease of the intensity of the strokes from the lowlands (< 100 *m* altitude) to the areas in the 100–200 *m* altitude belt. This could be determined by the influence of the sea as some thunderstorms developing over the sea can be advected towards the lowlands bringing marine characteristics of the strokes. As discussed in the previous section, strokes over the sea have larger currents compared to those over the land and this causes the current decrease from the lowlands compared to the areas in the 100–200 *m* altitude belt. However, further analyses are required to better disentangle this behaviour.

In the third panel, Fig. 7c, the average trend of current intensity for +CG (blue) and -CG (orange) as a function of ground altitude is shown. As expected, there is a gradual increase in intensities with increasing terrain altitudes.

So far, the analyses have been conducted without any temporal distinction but solely based on spatial classification. In the following section we will analyze the data according to a temporal classification, starting from yearly analysis and gradually moving towards monthly, daily and hourly analyses. We will also cross-reference the results with spatial distinctions to provide a more detailed analysis.

3.2. Temporal distribution

The temporal distribution analyses are conducted on an annual basis (section 3.2.1) over the 13-years long dataset. They are also performed on a seasonal basis, considering the four seasons (winter from December to February, spring from March to May, summer from June to August, and autumn from September to November), on a monthly basis for all 12 months of the year (section 3.2.2), and finally on a daily basis (section 3.2.3), considering the 24 h of the day in UTC format. The analyses are carried out on three parameters: the stroke density, the IC emission altitude, and the current intensity of the strokes.

3.2.1. Yearly analysis

Fig. 8 shows the yearly occurrence of total strokes (blue bars - left y-axis) together with the minimum current reported by the network (orange bars - right y-axis). On average we have 12.7 million strokes per year. The record peak of 28 million strokes is recorded in 2018, equivalent to over 18 strokes per km^2 for the entire year and there is a notable variability from year to year. The explanation is determined by the variability of meteorological events. The summer period of 2018 (4 months from May–August) recorded the highest number of strokes ever (almost 22 out of 28 million for the whole year). In particular, August 2018 holds the absolute record among all the months analyzed with

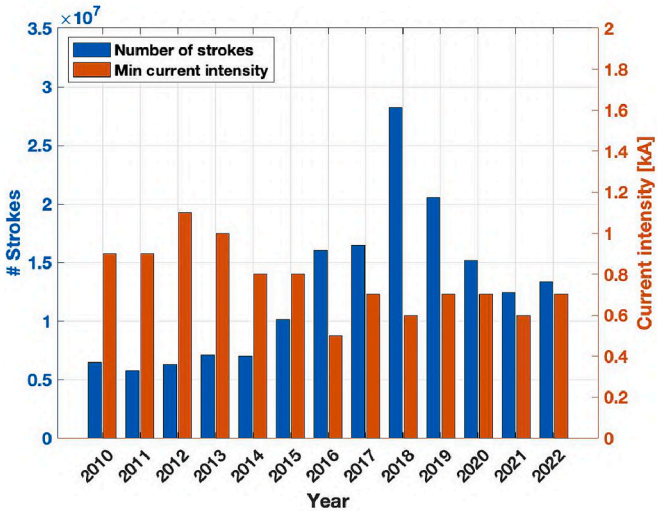

Fig. 8. Yearly distribution of the number of strokes reported in the entire domain (blue bars) and the respective minimum current reported by the lightning detection network (orange bars). (For interpretation of the references to colour in this figure legend, the reader is referred to the web version of this article.)

almost 9 million strokes. June 2018 with almost 6 million strokes is the 3rd month overall. Looking at a daily level, the 14*th* August 2018 holds the absolute record among all days with 1.4 million strokes in a single day and in second place overall is 8*th* June of the same year with 1.2 million. It follows that in 2018 there were actually several meteorological events with an exceptional number of strokes. However, the growth in strokes recorded until 2018 did not continue in the following years, suggesting that there is no clear trend in the number of strokes recorded in the last decade.

3.2.2. Monthly-Seasonal analysis

The monthly distribution of the number of strokes shown in Fig. 9 confirms what is well known from the literature, namely that the highest number of strokes is recorded in the warmer months, reaching its peak in

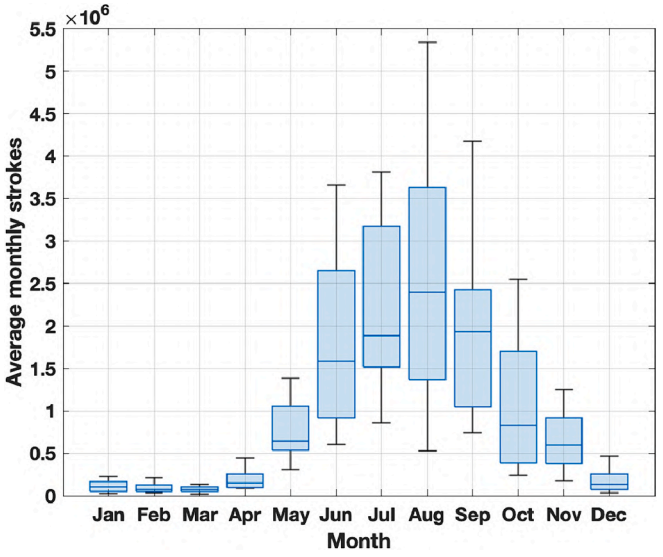

Fig. 9. Monthly distribution of strokes recorded across the entire domain. Each box encloses the 1*st* and 3*rd* quartiles of the number of strokes recorded in the respective month, with the blue line in the middle representing the median value. (For interpretation of the references to colour in this figure legend, the reader is referred to the web version of this article.)

August with an average of $2.4 * 10^6$ strokes, and the lowest value occurs in February/March with 0.7×10^5 strokes. Focusing on the variability of individual months, it can be observed that March has the lowest variability in the number of strokes, with a standard deviation of 5×10^4 strokes. On the other hand, the maximum variability is observed in August, where the standard deviation is 2.3×10^6 strokes. Examining the threshold corresponding to the 1*st* quartile, it is noted that in July, more frequently than in any other month, a high number of strokes exceeds the threshold of 1.5 million.

From June to September, there is a significant increase of lightning activity with respect to other months: 74% of electrical discharges are concentrated in these four months of the year. A total of 58% of lightning strokes occur during the summer season and August counts the 22.4% of the total.

In Fig. 10, the normalized monthly distribution of strokes over land (orange bars) and over sea (blue bars) is shown. Two different normalization modes are provided: on the panel a, relative to the total strokes for each surface, to observe the monthly-trend over different surfaces, and on the panel b, relative to each individual month, to compare the monthly distribution over sea and land.

In the top panel a, it can be observed that strokes over land are more frequent during summertime with the maximum peak occurring in July. The graph shows that the combined contributions from land and sea result in the overall maximum of detected strokes in August, as previously observed in Fig. 9.

The temporal shift of the convection from the land to sea from summer to autumn is apparent; similarly, in spring the convection shifts again from the sea to the land. This behaviour is even better represented in the bottom panel b, where the fraction of strokes is computed for different months. So, in summer the convection activity reaches its peak because of the surface warming that is able to trigger convection in a potentially unstable atmosphere. In addition, breezes can develop and organise convection in the lowlands or in the slopes of the mountains. The latent heat plays also a role both after the convection is triggered by the surface warming or when a synoptic scale storms enters the central Mediterranean in summer. The situation changes drastically in autumn and other months: in this case the convection is mainly forced over the sea due to the fact that the sea surface is warmer compared to the overlying atmosphere and the convection develops when fresh air is advected over the sea. So, there are two dominant forcings: the solar heating in summer and the warm sea surface in other seasons. Of course, this occurs on average; the solar heating can be important for some events in autumn, and synoptic and sub-synoptic scale storms can occur in summer as well.

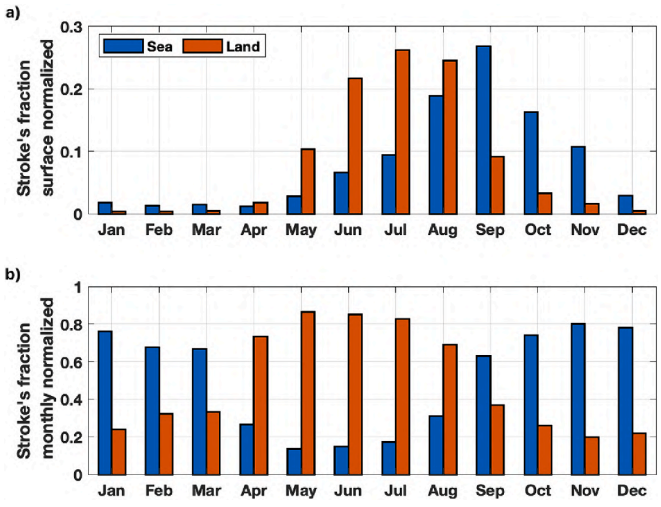

Fig. 10. Monthly distribution of strokes detected over sea (blue) and over land (orange), normalized relative to the total number of strokes for each surface (panel a) and relative to each individual month (panel b). (For interpretation of the references to colour in this figure legend, the reader is referred to the web version of this article.)

To further analyze the monthly distributions, the months of February, May, July and September are analyzed more in detail (Fig. 11). It can be observed that in February there are generally few strokes, primarily concentrated over the sea and at lower latitudes. In May, the spatial coverage of strokes is extensive, with a clear prevalence over the land. This is a consequence of the surface heating, which is able to trigger the convection in potentially unstable environments. Interestingly, in May it is well apparent the maximum of the strokes' density in NE Italy. The role of the surface warming becomes more significant and the convection dominates the northern part of Italy and the Italian mainland. In July the maximum over Liguria is apparent, aided by the organization of the circulation by the sea-breeze and mountain-valley flows (Federico et al. (2000); Holler et al. (2009)). Interestingly, there is a maximum in the northern Adriatic Sea, likely determined by the storms that develop over the land and then propagates over the sea. These storms decrease from north to south, as apparent by the strokes' distribution over the Italian peninsula. This gradient is not apparent in September, when colder air-masses are brought over the relative warm sea by the atmospheric circulation triggering the convection. For this reason, the strokes are rather widespread over both the Adriatic and Tyrrhenian Seas. In addition, it should be recalled the lower sensitivity of the LINET network going towards South and West of the domain (Fig. 6), which explains the small amount of stokes over the Mediterranean Sea, north of Tunisia and Algeria. Finally, it is well apparent a local maximum in the strokes density west of Tuscany and Lazio regions. This rather intense activity is caused by storms that originate over the sea in this season and propagate landwards, following the main circulation (Federico et al. (2014, 2019)).

Fig. 12 displays the monthly trend of strokes recorded over land across the 7 ground levels, normalized according to the ground altitude. As previously noticed, it is evident that the month of July exhibits the highest number of strokes at each altitude level, followed by August. Particularly, over 40% of the strokes occurring in high mountain areas are recorded in July. Another interesting result is that in other months lightning activity is more pronounced at lower ground levels. Stated in other terms, the summer convection is not only more intense compared to other seasons but tends to shift to higher altitudes. On the contrary, in other seasons, lightning prevails at lower altitudes. This behaviour in summer is caused by the higher energy available for convection and by the rising of the charging zone (especially in July and August).

As a final monthly analysis, let's consider the trend of stroke currents based on the type of surface. Fig. 13 illustrates the monthly variation of average current intensities for strokes recorded over sea (blue line), land (orange line), and the whole domain (black line). Strokes recorded over sea exhibit the highest average current intensities throughout the year, while those over land show the weakest intensities. The trend of current intensities for strokes is similar regardless of the surface type: on average, the most intense strokes occur in January (20.9 *kA* over sea and 17.4 *kA* over land); the weakest strokes are observed in summer, specifically in June (7.3 *kA*) over land and in July (8.4 *kA*) over sea.

In general, strokes with the highest current intensities are recorded in the cold months, particularly in January with average values exceeding 20 *kA*. Conversely, strokes with the least intense currents are found during the warm periods, with the minimum value occurring in July at only 7.6 *kA*. Similar results were found by Poelman et al. (2016) using the EUCLID network across Europe and by Brook (1992) in the United States. This behaviour is likely determined by the atmospheric turbulence intensity, which is higher in summer and over the land compared to other seasons and over the sea. The turbulence reduces the distance between pockets of opposite charges, intensifying the local electric field and facilitating the breakdown. When the turbulence is more intense, more strokes are generated and their currents are lower because they are produced by relative smaller pockets of charges.

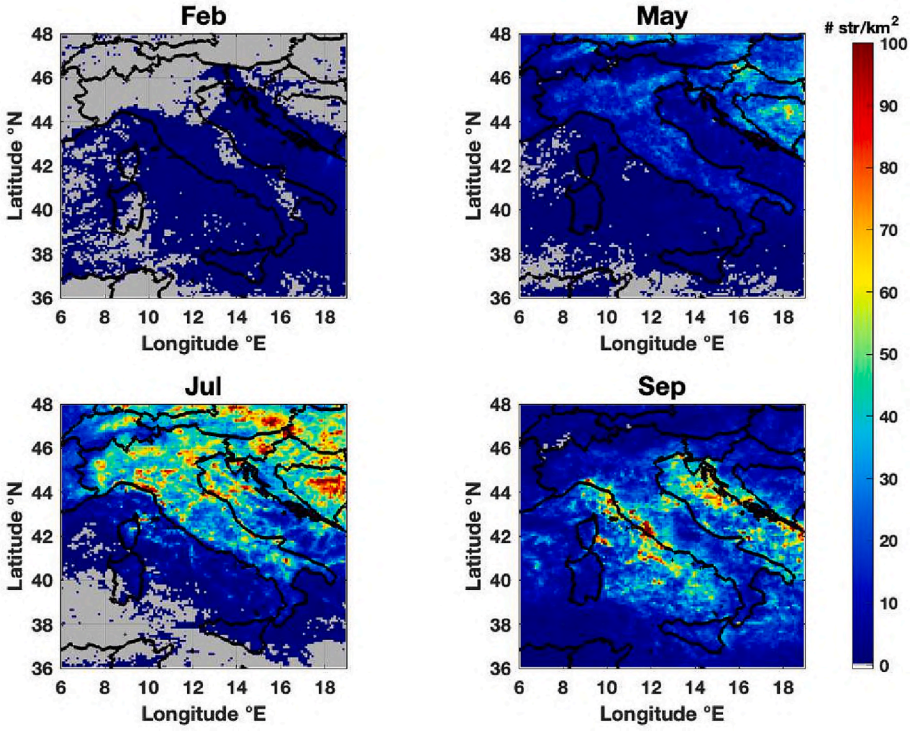

Fig. 11. Spatial distribution of strokes in four months which correspond to the annual minimum (February), maximum land coverage of strokes (May), peak maximum over land (July), and maximum stroke count over sea areas (September).

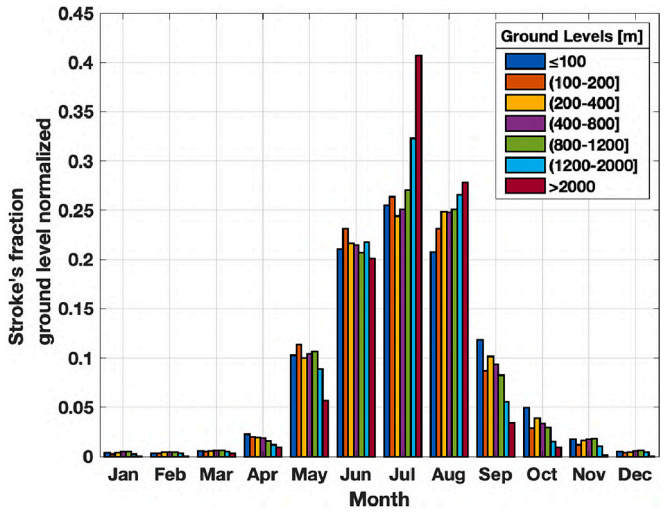

Fig. 12. Monthly distribution of strokes detected in the 7 ground levels, normalized according to the altitude level.

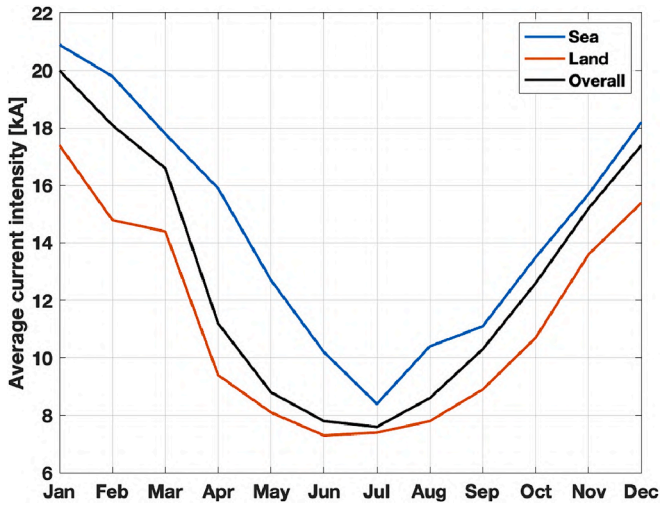

Fig. 13. Monthly trend of average stroke current intensities for different surface types.

3.2.3. *Diurnal cycle*

In this section we examine the distribution of strokes throughout the daily hours, covering the 24-h period. As extensively documented in literature, it is observed that afternoon thunderstorms (heat-induced) represent the main source of lightning. As shown in Fig. 14, the peak of total strokes occurs in the afternoon at 15:00 UTC (i.e., between 14:00 and 15:00 UTC), with a total of 13.1×10^6 strokes, equivalent to 8% of the daily strokes and double the hourly average. The period between 11:00 and 20:00 UTC concentrates 57% of the daily strokes, while the central afternoon hours (between 13:00 and 17:00 UTC) account for 30% of the data. The minimum number of strokes, merely 4.2×10^6, representing 2.57%, occurs at 02:00 UTC. It is worth noting that a secondary relative peak is observed at 05:00 UTC, during the early morning hours. The breakdown of contributions between strokes over land and over sea reveals that this secondary peak is primarily driven by strokes recorded over the sea: during the early hours of the day, only one-third of strokes occur over land, while the rest occur over sea. In the afternoon, however, lightning activity is predominantly concentrated over land (Fig. 14a). However, the most prominent difference between sea and land is the much smaller diurnal cycle over the sea. This result is expected considering that the strokes in the afternoon occur mainly over land being caused by the summer convection forced by the solar heating. The diurnal cycle over the sea is more complex: first, it is much smaller in the afternoon because of the much larger specific heat capacity of the sea; second, the maximum activity in the early morning is caused by the cooler air masses advected from the land to the sea in these hours of the

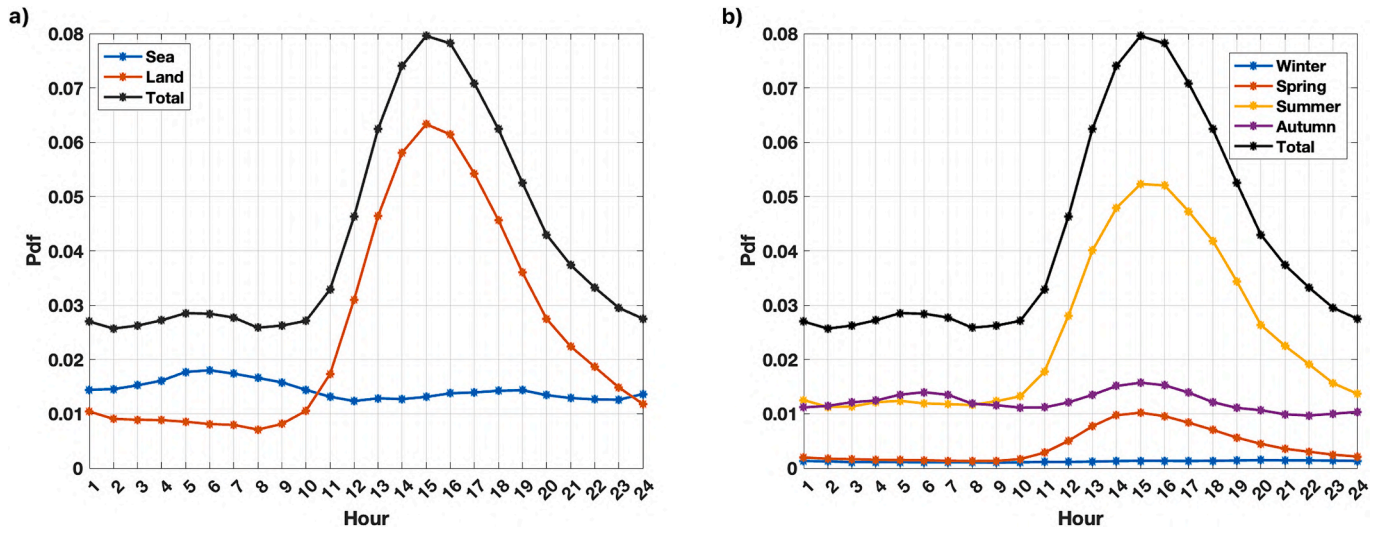

Fig. 14. Hourly pdfs. Panel **a**: Daily strokes detected over the sea (blue) and over the land (orange) areas. Panel **b**: daily seasonal strokes: winter (blue), spring (orange), summer (yellow) and Autumn (purple). The total strokes recorded in each hour is indicated in black. (For interpretation of the references to colour in this figure legend, the reader is referred to the web version of this article.)

morning.

The above analysis is confirmed by the seasonal contribution shown in the panel b, in which we can observe that the peak in the afternoon is primarily attributed to summer thunderstorms (with a secondary contribution from autumn and spring thunderstorms), while the secondary peak during the early morning in autumn slightly prevails compared to summer. On the other hand, the winter period provides a minimal contribution to the total lightning with no significant variations throughout the day.

This is shown in the panels of Fig. 15, which depict the spatial distributions of strokes in the four seasons detected at 05:00 UTC (on the left) and 15:00 UTC (on the right). At 05:00 UTC, we observe that in winter and spring, there are few strokes, mainly occurring over the sea. In summer, there is a high number of strokes concentrated over land, but with significant activity over the sea as well. In autumn, the distribution of strokes is predominantly over the sea, indicating notable electrical activity during the early hours of the day.

Even looking at strokes distribution at 15:00 UTC, the winter season still shows a low occurrence confirming the low daily variability of strokes during this season. In spring afternoons, the distribution of strokes is mainly concentrated over land, except for the Alpine ridge. In summer, the highest number of afternoon strokes is observed over land. Note also the electrical activity over the Adriatic Sea, which is determined by the advection of summer thunderstorms from the surrounding lands towards the Sea. Finally, in autumn, the strokes occur with the same frequency over land and over sea.

The daily variation of stroke current intensities shows very interesting features. In Fig. 16a, the daily variation of currents for strokes identified over the sea (blue line), over land (orange line), and over the entire domain (black line) is shown. As previously observed, the behaviour of daily currents is also not the same for different surface types. The black curve represents the overall trend, with maximum intensity values occurring during the nighttime hours (11.8 *kA* at 02:00 UTC) and minimum values during the afternoon hours (8.2 *kA* between 15:00 and 17:00 UTC). The same trend is observed over land, with values consistently lower than those recorded over sea, as previously seen. On average, over the land, the intensity values range from 7.2 to 9.9 *kA*, with the maximum occurring during the nighttime and the minimum in the late afternoon. Over the sea, however, the values are significantly higher, ranging from 11.4 to 13.1 *kA*. Nonetheless, the trend exhibits a sinusoidal curve with two main peaks and two troughs, although the main trough and peak appear to be in phase with their

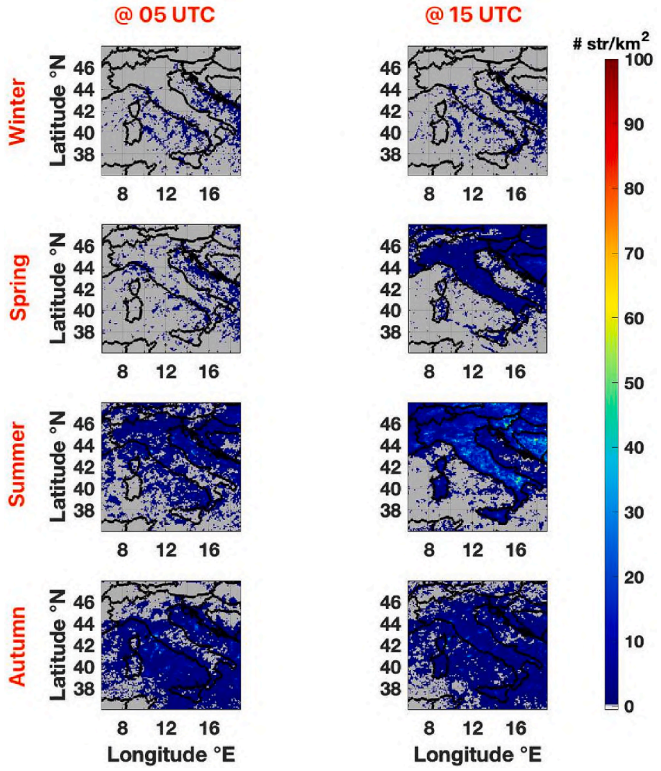

Fig. 15. The spatial distribution of strokes during the four seasons is shown on the left at 05:00 UTC (corresponding to the period between 04:00 and 05:00 UTC, representing the second relative daily maximum) and on the right at 15:00 UTC (corresponding to the period between 14:00 and 15:00 UTC, representing the daily peak).

counterparts over land (i.e., the trough in the afternoon and the peak during the nighttime). The diurnal cycle of the currents over land is further analyzed by examining the variations at different ground altitudes, as shown in Fig. 16b. The hourly variation of current intensities is displayed for the seven ground altitude levels. At all elevations, a clear daily trend is observed: there is a minimum in intensity during the late afternoon (around 18:00 UTC) and a maximum during the nighttime

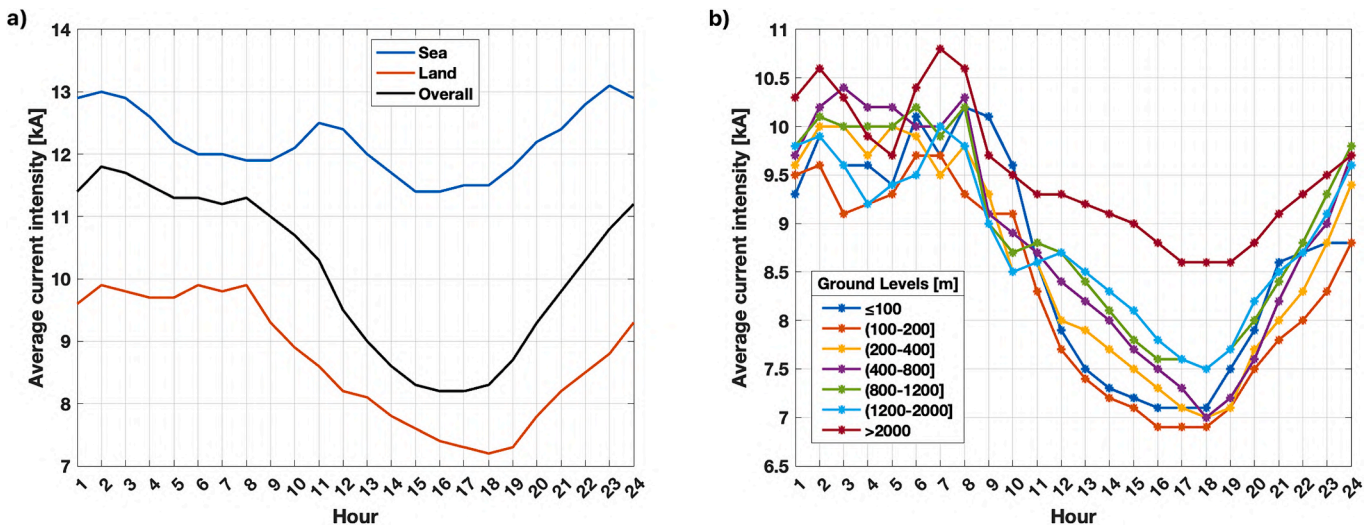

Fig. 16. The daily variation of stroke current intensities classified by surface type (panel **a**) and by different ground altitudes (panel **b**).

hours.

The unique daily pattern of stroke intensities over land was first studied by Chronis et al., 2015, who, however, did not definitively identify the causes (still unknown) that could explain this behaviour. The results of their study offer evidence that the variation in peak current is primarily influenced by the diurnal pattern of stroke activity. Afternoon and evening thunderclouds, known for their higher CG rates, exhibit stronger generator currents, indicating a more intense electrification process driven by precipitation. These thunderclouds are characterized by stronger vertical updraft speeds and higher cloud tops (Williams (1985); Blakeslee et al. (1989); Mach et al. (2011)).

Considering the presence of a more robust precipitation mechanism in the afternoon thunderclouds, it is reasonable to argue a higher abundance of ice particles (such as graupel and ice crystals) and other charged hydrometeors within the thundercloud. These particles effectively diminish the electric field required for thundercloud breakdown, particularly when compared to the comparatively less active morning thundercloud (Petersen et al. (2008)).

Additionally, the increased turbulent mixing within the late afternoon thundercloud fosters the convergence of pockets of opposite charges in closer proximity. As a result, locally intensified electric fields form, facilitating the occurrence of "premature" breakdown and enhancing the initiation of lightning (Bruning and MacGorman (2013)).

The net result is that the lower flash rates during morning storms contribute to the formation of larger charge centers compared to late afternoon storms. This leads to a greater availability of charge for the strokes. Observations of electric fields below and above thunderstorms support the notion that weaker storms exhibit thundercloud fields and associated charge centers with substantial amplitudes. Therefore, it is reasonable to expect smaller peak currents during periods of high CG rates (Chronis et al. (2015)).

4. Conclusions

In this paper, we presented the first comprehensive study of IC and CG strokes from the LINET network over a large area of nearly 1.5 million km^2, centered around the Italian peninsula and including parts of the neighboring European countries and the central Mediterranean Sea. We analyzed the spatial and temporal distribution and characteristics of >165 million strokes recorded over a 13-year period from 2010 to 2022, resulting in an average of 8.14 strokes/km^2/yr. We verified a higher average density of strokes than any previous study conducted in the same area, indicating the network's high sensitivity to lower stroke intensities. The main conclusions can be summarized as follows:

- The stroke intensities range from 0.5 to 600 *kA* (in magnitude). Positive discharges, such as IC, are generally weaker and limited in their range, while negative discharges have higher intensities. Strokes' intensities are lower over land compared to the sea but increase with terrain altitude. A strong seasonal correlation is observed for average intensities, with minimum values in summer (July, 7 *kA*) and maximum values in winter (January, 21 *kA*).
- A pronounced correlation is observed during daily trends over land, with lower average intensities recorded in the late afternoon and higher values during nighttime.
- The average height of IC emission ranges between 7 and 8 *km*, with 75% of strokes occurring below 9.8 *km*. The discharge altitude is weakly dependent on the type of surface, with higher altitudes over sea and lower altitudes over land. This behaviour is partially determined by the lower sensitivity of the LINET network over the sea.
- Over land, the orography significantly influences the discharge altitude and the vertical development of cumulonimbus clouds. Seasonally, important trends are observed, with maximum discharge altitudes in summer and minimum altitudes in winter.
- The density of strokes is higher over land compared to sea, with some regions showing higher activity than others due to orographic factors and, maybe, to anthropogenic activities as pollution increases the local electric field and could enhance the strokes density.
- The density of discharges decreases with increasing terrain altitude, and correspondingly, the percentage of negative discharges increases.
- The lightning season spans from May to October, concentrating 90% of the total lightning activity: the peak of thunderstorms is observed over the land in July and over the sea in September, with the overall maximum occurring in August (22%) when considering both contributions. There is a substantial change of the strokes pattern between summer and autumn. In summer, strokes are mainly located over land, in autumn they occur mainly over the sea.

CRediT authorship contribution statement

Marco Petracca: Writing – original draft, Software, Methodology, Formal analysis, Data curation, Conceptualization. **Stefano Federico**: Writing – original draft, Methodology, Conceptualization, Writing – review & editing. **Nicoletta Roberto:** Writing – review & editing, Methodology, Conceptualization. **Silvia Puca:** Writing – review & editing, Conceptualization. **Leo Pio D'Adderio:** Writing – review & editing, Writing – original draft, Methodology, Conceptualization. **Rosa Claudia Torcasio:** Writing – review & editing, Writing – original draft,

Methodology, Conceptualization. **Stefano Dietrich:** Writing – review & editing, Writing – original draft, Methodology, Formal analysis, Conceptualization.

Declaration of competing interest

The authors declare that they have no known competing financial interests or personal relationships that could have appeared to influence the work reported in this paper.

Data availability

The authors do not have permission to share data.

Acknowledgements

This work was made possible thanks to the agreement between the Institute of Atmospheric and Climate Sciences of the CNR and Nowcast GmbH. We would like to express our gratitude to Nowcast GmbH for making available the data of the European lightning network LINET, which is essential for our analysis. More information about their services and products are available on website https://www.nowcast.de/en/.

Appendix A. 1 MyLightning Database

CNR-ISAC collects, organizes, and manages lightning data from the LINET network in the Central part of the Mediterranean area since January 2010. Up today, over 7 million of files (1 file per minute) are stored and analyzed. The data are acquired in NRT and organized in MyLightning DB for statistical and scientific research purposes. MyLightning is a DB based on the SQL system which is constantly updated with strokes data detected from the LINET network in NRT. Every minute a new record is created in the table "minutes" which contains all LINET file information. In a LINET file, each line provides a description of a single stroke reporting temporal information (i.e., year, month, day, hour, minute, second, and thousandths of a second). It also includes spatial information, such as the north latitude and east longitude coordinates of the electric discharge. In addition, the discharge altitude (expressed in *km*), the type of discharge (1 = CG or 2 = IC), the intensity of the discharge (in *kA*), and a quality parameter related to the measurement are also reported.

The file is decompressed, opened, checked, read and all stroke parameters contained are imported into the table "strokes". Subsequently, a series of statistical scores are computed to classify, catalog and highlight the strokes and the lightnings characteristics. MyLightning currently counts >30 tables, 250 millions of records, for the most part containing statistical results on strokes and on files archived.

For the present study, it is important to know the confidence level of the statistical results, i.e. verify the percentage of completeness of the whole DB. Considering the total number of files existing in the archive (during the 13 years analyzed), the DB is complete for 94.66%. This means that 5.34% of single minute files are not present in the archive for reasons attributable either to the failure to send (less likely) or to the failure to receive the file. This second possibility, the most probable, could be attributable to the impossibility of the host server to receive new data because power outages or internet connection or lack of storage space or other unknown causes. However this data loss has been greatly limited in recent years thanks to the achievement of a high-stability level of the whole system. Since 2016, in fact, the percentage of minutes recorded has been steadily increasing and in particular since 2019 it has constantly exceeded 99% for each year (99.43% completeness over the last 50 months). Based on the data availability, we are confident in the quality and consistency of the statistical results we presented in this study. Considering the above performance of the MyLightning database, an error of 5% should be considered in the statistics reported in this paper for the years before 2019. In any case, this error doesn't change appreciably any of the results presented.

References

Anderson, G., Klugmann, D., 2014. A european lightning density analysis using 5 years of atdnet data. Nat. Hazards Earth Syst. Sci. 14 (4), 815–829.

Aranguren, D., López, J., Inampués, J., Torres, H., Betz, H., 2014. Cloud to ground ligthning activity in colombia and the influence of topography. In: 2014 International Conference on Lightning Protection 2014, pp. 182–189. URL. https://ieeexplore.ieee.org/document/6973430.

Aranguren, D., López, J., Inampués, J., Torres, H., Betz, H., 2017. Cloud-to-ground lightning activity in Colombia and the influence of topography. J. Atmos. Sol. Terr. Phys. 154, 182–189.

Avolio, E., Federico, S., 2018. Wrf simulations for a heavy rainfall event in southern Italy: Verification and sensitivity tests. Atmos. Res. 209, 14–35.

Betz, H.-D., Schmidt, K., Oettinger, P., Wirz, M., 2004. Lightning detection with 3-d discrimination of intracloud and cloud-to-ground discharges. Geophys. Res. Lett. 31 (11).

Betz, H.D., Schmidt, K., Laroche, P., Blanchet, P., Oettinger, W.P., Defer, E., Dziewit, Z., Konarski, J., 2009. Linet—an international lightning detection network in europe. Atmos. Res. 91 (2), 564–573.

Blakeslee, R.J., Christian, H.J., Vonnegut, B., 1989. Electrical measurements over thunderstorms. J. Geophys. Res. Atmos. 94 (D11), 13135–13140.

Bond, D.W., Steiger, S., Zhang, R., Tie, X., Orville, R.E., 2002. The importance of nox production by lightning in the tropics. Atmos. Environ. 36 (9), 1509–1519.

Brook, M., 1992. Breakdown electric fields in winter storms. J. Atmospheric Electricity 12 (1), 47–52.

Bruning, E.C., MacGorman, D.R., 2013. Theory and observations of controls on lightning flash size spectra. J. Atmos. Sci. 70 (12), 4012–4029.

Buiat, M., Porcù, F., Dietrich, S., 2017. Observing relationships between lightning and cloud profiles by means of a satellite-borne cloud radar. Atmos. Meas. Tech. 10 (1), 221–230.

Cacciamani, C., Battaglia, F., Patruno, P., Pomi, L., Selvini, A., Tibaldi, S., 1995. A climatological study of thunderstorm activity in the po valley. Theor. Appl. Climatol. 50, 185–203.

Christian, H.J., Blakeslee, R.J., Boccippio, D.J., Boeck, W.L., Buechler, D.E., Driscoll, K. T., Goodman, S.J., Hall, J.M., Koshak, W.J., Mach, D.M., Stewart, M.F., 2003. Global frequency and distribution of lightning as observed from space by the optical transient detector. J. Geophys. Res. Atmos. 108 (D1). ACL 4–1–ACL 4–15.

Chronis, T., Cummins, K., Said, R., Koshak, W., McCaul, E., Williams, E.R., Stano, G.T., Grant, M., 2015. Climatological diurnal variation of negative cg lightning peak current over the continental United States. J. Geophys. Res. Atmos. 120 (2), 582–589.

Curran, E.B., Holle, R.L., López, R.E., 2000. Lightning casualties and damages in the United States from 1959 to 1994. J. Clim. 13 (19), 3448–3464.

De Pablo, F., Soriano, L.R., 2002. Relationship between cloud-to-ground lightning flashes over the iberian peninsula and sea surface temperature. Q. J. R. Meteorol. Soc. 128 (579), 173–183.

Deierling, W., Petersen, W.A., Latham, J., Ellis, S., Christian, H.J., 2008. The relationship between lightning activity and ice fluxes in thunderstorms. J. Geophys. Res. 113.

Diendorfer, G., Bernardi, M., Cummins, K., La Rosa, F., Hermoso, B., Hussein, A., Kawamura, T., Rachidi, F., Rakov, V., Schulz, W., Torres, H., 2009. Cloud to ground lightning parameters derived from lightning detection systems. The effects of the performance. CIGRE Technical Brochure 376.

Federico, S., Dalu, G.A., Bellecci, C., Colacino, M., 2000. Mesoscale energetics and flows induced by sea-land and mountain-valley contrasts. Ann. Geophys. 18 (11), 235–246.

Federico, S., Avolio, E., Pasqualoni, L., De Leo, L., Sempreviva, A.M., Bellecci, C., 2009. Preliminary results of a 30-year daily rainfall data base in southern Italy. Atmos. Res. 94 (4), 641–651 (precipitation science: measurement, remote sensing, climatology and modelling).

Federico, S., Avolio, E., Petracca, M., Panegrossi, G., Sanò, P., Casella, D., Dietrich, S., 2014. Simulating lightning into the rams model: implementation and preliminary results. Nat. Hazards Earth Syst. Sci. 14 (11), 2933–2950.

Federico, S., Torcasio, R.C., Avolio, E., Caumont, O., Montopoli, M., Baldini, L., Vulpiani, G., Dietrich, S., 2019. The impact of lightning and radar reflectivity factor data assimilation on the very short-term rainfall forecasts of rams@isac: application to two case studies in Italy. Nat. Hazards Earth Syst. Sci. 19 (8), 1839–1864.
Feudale, L., Manzato, A., 2014. Cloud-to-ground lightning distribution and its relationship with orography and anthropogenic emissions in the po valley. J. Appl. Meteorol. Climatol. 53 (12), 2651–2670.
Flaounas, E., Davolio, S., Raveh-Rubin, S., Pantillon, F., Miglietta, M.M., Gaertner, M.A., Hatzaki, M., Homar, V., Khodayar, S., Korres, G., Kotroni, V., Kushta, J., Reale, M., Ricard, D., 2022. Mediterranean cyclones: current knowledge and open questions on dynamics, prediction, climatology and impacts. Weather and Climate Dynamics 3 (1), 173–208.
Galanaki, E., Flaounas, E., Kotroni, V., Lagouvardos, K., Argiriou, A., 2016. Lightning activity in the mediterranean: quantification of cyclones contribution and relation to their intensity. Atmos. Sci. Lett. 17 (9), 510–516.
Galanaki, E., Lagouvardos, K., Kotroni, V., Flaounas, E., Argiriou, A., 2018. Thunderstorm climatology in the mediterranean using cloud-to-ground lightning observations. Atmos. Res. 207, 136–144.
Holle, R.L., 2008. Annual rates of lightning fatalities by country. In: 20th International Lightning Detection Conference, 21–23 April 2008, and the 2nd International Lightning Meterology Conference, 24–25 April 2008. Tuscon, Arizona.
Holler, H., Betz, H.-D., Schmidt, K., Calheiros, R.V., May, P., Houngninou, E., Scialom, G., 2009. Lightning characteristics observed by a vlf/lf lightning detection network (linet) in Brazil, Australia, africa and Germany. Atmos. Chem. Phys. 9 (20), 7795–7824.
Holt, M.A., Hardaker, P.J., McLelland, G.P., 2001. A lightning climatology for europe and the Uk, 1990–99. Weather 56 (9), 290–296.
Kotroni, V., Lagouvardos, K., 2008. Lightning occurrence in relation with elevation, terrain slope, and vegetation cover in the mediterranean. J. Geophys. Res. Atmos. 113 (D21).
Kotroni, V., Lagouvardos, K., 2016. Lightning in the mediterranean and its relation with sea-surface temperature. Environ. Res. Lett. 11.
Mach, D.M., Blakeslee, R.J., Bateman, M.G., 2011. Global electric circuit implications of combined aircraft storm electric current measurements and satellite-based diurnal lightning statistics. J. Geophys. Res. Atmos. 116 (D5).
Manzato, A., Serafin, S., Miglietta, M., Kirshbaum, D., Schulz, W., 2022. A pan-alpine climatology of lightning and convective initiation. Mon. Weather Rev. 150, 2213–2230.
Mohr, S., Wandel, J., Lenggenhager, S., Martius, O., 2019. Relationship between atmospheric blocking and warm-seas on thunderstorms over western and central europe. Quart. J. Roy.Meteor. Soc. 145, 3040–3056.
Naccarato, K., Pinto, O., Pinto, I., 2003. Evidence of thermal and aerosol effects on the cloud-to-ground lightning density and polarity over large urban areas of outheastern Brazil. Geophys. Res. Lett. 30.
Nag, A., Murphy, M.J., Schulz, W., Cummins, K.L., 2015. Lightning locating systems: Insights on characteristics and validation techniques. Earth and Space Sci. 2 (4), 65–93.
Nesbitt, S.W., Zhang, R., Orville, R.E., Jan 2000. Seasonal and Global nox Production by Lightning Estimated from the Optical Transient Detector (Otd). Chemical and Physical Meteorology, Tellus B.
Orville, R.E., Huffines, G., Nielsen-Gammon, J., Zhang, R., Ely, B., Steiger, S., Phillips, S., Allen, S., Read, W., 2001. Enhancement of cloud-to-ground lightning over Houston, Texas. Geophys. Res. Lett. 28 (13), 2597–2600.
Petersen, W.A., Rutledge, S.A., 1998. On the relationship between cloud-to-ground lightning and convective rainfall. J. Geophys. Res. Atmos. 103 (D12), 14025–14040.
Petersen, D., Bailey, M., Beasley, W.H., Hallett, J., 2008. A brief review of the problem of lightning initiation and a hypothesis of initial lightning leader formation. J. Geophys. Res. Atmos. 113 (D17).
Petracca, M., D'Adderio, L.P., Porcù, F., Vulpiani, G., Sebastianelli, S., Puca, S., 2018. Validation of gpm dual-frequency precipitation radar (dpr) rainfall products over Italy. J. Hydrometeorol. 19 (5), 907–925.
Piper, D., Kunz, M., 2017. Spatiotemporal variability of lightning activity in europe and the relation to the North Atlantic oscillation teleconnection pattern. Nat. Hazards Earth Syst. Sci. 17 (8), 1319–1336.
Poelman, D.R., Schulz, W., Diendorfer, G., Bernardi, M., 2016. The european lightning location system Euclid – part 2: Observations. Nat. Hazards Earth Syst. Sci. 16 (2), 607–616.
Pohjola, H., Mäkelä, A., 2013. The comparison of gld360 and Euclid lightning location systems in europe. In: Atmospheric Research 123, 117–128, 6th European Conference on Severe Storms 2011. Palma de Mallorca, Spain.
Reeve, N., Toumi, R., 1999. Lightning activity as an indicator of climate change. Q. J. R. Meteorol. Soc. 125 (555), 893–903.
Roberto, N., Adirosi, E., Baldini, L., Casella, D., Dietrich, S., Gatlin, P., Panegrossi, G., Petracca, M., Sanò, P., Tokay, A., 2016. Multi-sensor analysis of convective activity in Central Italy during the hymex sop 1.1. Atmospheric. Meas. Tech. 9 (2), 535–552.
Schultz, W., Diendorfer, G., Pedeboy, S., Poelman, D.R., 2016. The european lightning location system Euclid - part i: Performance analysis and validation. Nat. Hazards EarthSyst. Sci. 16 (2), 595–605.
Sokol, Z., Popová, J., Skripniková, K., Torcasio, R.C., Federico, S., Fišer, O., 2023. Comparison of cloud structures of storms producing lightning at different distance based on five years measurements of a doppler polarimetric vertical cloud profiler. Remote Sens. 15 (11). URL. https://www.mdpi.com/2072-4292/15/11/2874.
Taszarek, M., Allen, J., Púčik, T., Groenemeijer, P., Czernecki, B., Kolendowicz, L., Lagouvardos, K., Kotroni, V., Schulz, W., 2019. A climatology of thunder-storms across europe from a synthesis of multiple data. J. Clim. 32, 1813–1837.
Torcasio, R.C., Papa, M., Del Frate, F., Dietrich, S., Toffah, F.E., Federico, S., 2023. Study of the intense meteorological event occurred in september 2022 over the Marche region with wrf model: Impact of lightning data assimilation on rainfall and lightning prediction. Atmosphere 14 (7).
Virts, K.S., Wallace, J.M., Hutchins, M.L., Holzworth, R.H., 2013. Highlights of a new ground-based, hourly global lightning climatology. Bull. Am. Meteorol. Soc. 94 (9), 1381–1391.
Wierzchowski, J., Heathcott, M., Flannigan, M.D., 2002. Lightning and lightning fire, central cordillera, Canada. Int. J. Wildland Fire 11, 41–51.
Williams, E.R., 1985. Large-scale charge separation in thunderclouds. J. Geophys. Res. Atmos. 90 (D4), 6013–6025.
Wu, F., Cui, X., Zhang, D.-L., Liu, D., Zheng, D., 2016. Safir-3000 lightning statistics over the Beijing metropolitan region during 2005–07. J. Appl. Meteorol. Climatol. 55 (12), 2613–2633.
Xu, M., Qie, X., Pang, W., Shi, G., Liang, L., Sun, Z., Yuan, S., Zhu, K., Zhao, P., 2022. Lightning climatology across the chinese continent from 2010 to 2020. Atmos. Res. 275, 106251.
Zhang, W., Zhang, Y., Zheng, D., Xu, L., Lyu, W., 2018. Lightning climatology over the northwest pacific region: an 11-year study using data from the world wide lightning location network. Atmos. Res. 210, 41–57.